Experimental Animals
Exp. Anim. 70(2), 225–235, 2021

Original

Establishment and histopathological study of patient-derived xenograft models and primary cell lines of epithelioid malignant peritoneal mesothelioma

Zhi-Ran YANG[1)], Zhi-Gao CHEN[2)], Zhong-He JI[1)], Yu-Lin LIN[1)], Jue ZHANG[1)], Ru MA[1)], Zhao LI[3)], Xi JIANG[3)], Qian CHEN[2)], Xue-Mei DU[3)], Yan LI[1,3)]

[1)]*Department of Peritoneal Cancer Surgery, Beijing Shijitan Hospital, Capital Medical University, No. 10 Tieyi Road, Yangfangdian Street, Haidian District, Beijing 100038, China*
[2)]*Thorgene Co., Ltd., Yizhuang Biomedical Park, Daxing District, Beijing, Beijing, China*
[3)]*Department of Pathology, Beijing Shijitan Hospital, Capital Medical University, Capital Medical University, No. 10 Tieyi Road, Yangfangdian Street, Haidian District, Beijing, China*

Abstract: Malignant peritoneal mesothelioma (MPM) is a rare malignancy with few experimental models. This study used the human surgical specimen to establish MPM patient-derived xenograft (PDX) models and primary cell lines to provide a study platform for MPM *in vitro* and *in vivo*, and conducted histopathological analysis. Our study used the experimental peritoneal cancer index (ePCI) score to evaluate gross pathology, and the results showed that the ePCI score of the female and male nude mice were 8.80 ± 1.75 and 9.20 ± 1.81 (P=0.6219), respectively. The Hematoxylin and eosin (HE) staining of animal models showed that the tumor was epithelioid mesothelioma and invaded multiple organs. Immunohistochemistry (IHC) staining showed that Calretinin, Cytokeratin 5/6, WT-1 and Ki-67 were all positive. The Swiss-Giemsa and Immunofluorescence (IF) staining of primary cell lines were also consistent with the pathological characteristics of mesothelioma. We also performed the whole-exome sequencing (WES) to identify the mutant genes between models and the patient. And the results showed that 21 mutant genes were shared between the two groups, and the genes related to tumorigenesis and development including *BAP1*, *NF2*, *MTBP*, *NECTIN2*, *CDC23*, *LRPPRC*, *TRIM25*, and *DHRS2*. In conclusion, the PDX models and primary cell lines of MPM were successfully established with the epithelioid mesothelioma identity confirmed by histopathological evidence. Moreover, our study has also illustrated the shared genomic profile between models and the patient.

Key words: histopathological study, malignant peritoneal mesothelioma, patient-derived xenograft (PDX) model, primary cell lines, whole exome sequencing

Introduction

Malignant peritoneal mesothelioma (MPM) is a rare malignancy characterized by highly malignant behavior and poor prognosis. MPM accounts for 10–30% of all malignant mesothelioma, and the median survival of patient ranged from 5 to 12 months [1, 2]. The Peritoneal Surface Oncology Group International (PSOGI) recommends the combination of cytoreductive surgery (CRS) with hyperthermic intraperitoneal chemotherapy (HIPEC) as the standard treatment [3, 4]. Although CRS+HIPEC could extend the median survival of patients to roughly 3 years, it proves little efficacy for some patients [5–7]. Therefore, it is urgent and necessary to

(Received 15 August 2020 / Accepted 13 December 2020 / Published online in J-STAGE 21 January 2021)
Corresponding author: Y. Li. e-mail: liyansd2@163.com

explore novel effective treatments for clinical improvement.

Animal models are important platforms for studying disease mechanisms and exploring new therapeutic strategies. Currently, there are mainly three types animal models of malignant mesothelioma, which including spontaneous models [8, 9], induced models [10], and transplanted models [11, 12]. The spontaneous models and induced models are the most similar to humans in terms of tumor occurrence, they reflect the susceptibility of animal tumors and the degree of aggregation of environmental carcinogens, and may help to discover environmental carcinogens. However, the disadvantages of these models limited its application, such as the different course of disease, the longer induction time, the lower induction rate, and unsuitable for drug screening. In contrast, the transplanted models are characterized by the shorter induction time, the higher induction rate, and suitable for conducting drug intervention experiments, thus the xenograft models are the most common tool for studying malignant mesothelioma.

The xenogeneic orthotopic transplant model of malignant pleural mesothelioma has been established, which simulated the clinical pathological process of the patient [13]. However, malignant pleural mesothelioma and MPM may have different gene expression profiles and genetic background [14, 15]. Therefore, it is requisite to establish xenograft models of MPM to further explore the mechanisms, discover new targets, and conduct drug screening study. Up to now, however, there has been few xenograft models of human MPM from China.

This study directly used surgical specimens to establish MPM patient-derived xenograft (PDX) models in nude mice, and primary cell lines. The major pathological features were also systematically studied.

Materials and Methods

Patient and tumor specimen

Tumor specimen was obtained from a 63-year-old female patient with no history of asbestos exposure and smoking. She complained of persistent abdominal pain for 4 months. Computed tomography (CT) of the abdomen showed effusion, diffuse abnormal enhancement nodules in the peritoneum and omentum, and multiple lymph nodes in the abdominal cavity. Cytology of effusion found the tumor cells, derived from mesothelium. The patient received CRS + HIPEC and was diagnosed as epithelial malignant peritoneal mesothelioma. Resected tumors were used for the establishment of PDX models. Informed consent has been obtained from the patient, and all experiments were performed under the guideline of the Scientific Research Ethics Committee of Beijing Shijitan Hospital, Capital Medical University [Approval number: 2020 Research Ethics Review No. (2)].

Animals

Specific pathogen free BALB/c *nu/nu* mice, 4–5 weeks old, 16–18 g, were purchased from Beijing Vital River Laboratory Animal Technology Co., Ltd. (Beijing, China) and were raised individually in ventilated cages in a barrier environment at the temperature of 20–26°C, in the humidity of 40–70% at Beijing Percans Oncology (Beijing, China). After a quarantine period of 7 days, mice were prepared for model establishment. The whole study procedures were illustrated in Fig. 1.

Establishment of MPM PDX models

Tumor specimens were washed with RPMI 1,640 medium (Corning, New York, NY, USA), cut into pieces sized of 1 mm^3, then inoculated subcutaneously on the back of nude mice using an inoculation needle with 2 mm diameter. The inoculation needle consists of an outer tube and a needle core, the outer tube was used to bluntly separate the subcutaneous (s.c.) connective tissue, and the tumor pieces can be injected into the s.c. space by pushing the needle core. The volume of s.c. tumors was measured every three days. When it reached 500 mm^3, the tumors were resected for characterization and passaging. The resected tumors were divided into five groups, including (1) histopathological study, (2) PDX model establishment, (3) primary cell culture, (4) s.c. inoculation on back of nude mice for passage, and (5) freeze preservation. The method of freeze preservation is as follows. The s.c. tumors were cut into pieces sized of 3 × 3 × 3 mm^3, and then placed in the preservation solution, which was composed of 60% RPMI 1640 medium, 30% fetal bovine serum (FBS; Gibco, Thermo Fisher, New York, NY, USA) and 10% dimethylsulfoxide (DMSO; Amresco, Framingham, MA, USA). The tumors were placed in Nalgene programmed cooling box (Thermo Fisher) at −80°C overnight and stored in liquid nitrogen. The frozen tumors were incubated at 37°C until complete melting when resuscitation. The s.c. models were reestablished using both fresh s.c. tumor tissue and frozen tumors. Two nude mice were inoculated each time.

After 4 passages, the fresh s.c. tumor was cut into pieces sized of 1 mm^3 and immersed in 1.5 ml RPMI 1,640 medium to produce 2.5 ml tumor tissue suspension. The tumor tissue suspension was placed in the outer tube of the inoculation needle. Disinfecting the skin at the injection site, separating the s.c. connective

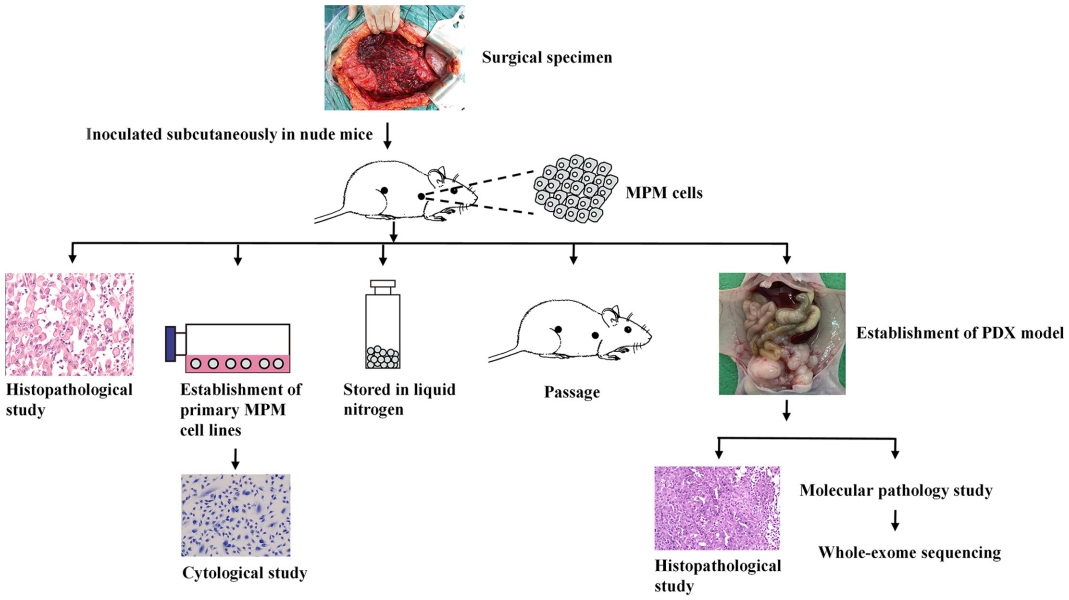

Fig. 1. Experimental procedures and histopathological analysis of the established malignant peritoneal mesothelioma (MPM) patient-derived xenograft (PDX) models and primary cell lines.

Table 1. Primary antibodies used for immunohistochemistry

Primary antibodies	Supplier	Catalog number	Dilution
rabbit anti-human Calretinin antibody	Zhongshan Golden Bridge	Poly	Ready to use
mouse anti-human WT-1 antibody	Genetic technology	6F-H2	Ready to use
mouse anti-human Cytokeratin 5/6 antibody	OriGene	OTI1C7	Ready to use
mouse anti-human Ki-67 antibody	OriGene	UMAB107	1:100

tissue with an outer tube, and then pushing the needle core of the inoculation needle to send the tumor tissues into the left lower abdominal cavity of the nude mice. 20 nude mice (10 males and 10 females) were used for MPM PDX model establishment. Each nude mouse was inoculated with 100 μl of tumor tissue suspension. Mice were closely monitored daily, with the body weight measured every three days.

Gross pathological study

Mice were euthanized with an intraperitoneal injection of euthanasia solution (150 mg/kg) containing sodium pentobarbital (390 mg/ml) and sodium phenytoin (50 mg/ml). At autopsy, the major organs were collected and recorded. Tumor growth and progression features were recorded. Experimental peritoneal cancer index (ePCI) was used to evaluate the extent of tumor dissemination, based on published studies by Lin [16]. The abdominal-pelvic cavity was divided into 4 subareas, and lesion size score (LS) in each subarea is determined by the diameter of the largest tumor: LS-0, no visible tumor; LS-1, diameter $\leq$ 0.2 cm; LS-2, 0.2 cm < diameter $\leq$ 0.5 cm; LS-3, diameter > 0.5 cm; Malignant ascites, 1 point. The accumulative ePCI score ranges from 0 to 13.

Histopathological study

Tumor and organ tissues were fixed in 4% formaldehyde solution for 48 h, followed by routine dehydration, paraffin embedding and section (4 μm). Hematoxylin-eosin (HE) staining (Dako Hematoxylin, Dako Eosin and Dako Bluing Buffer, catalog number CS701) was performed on Dako CoverStainer (Agilent Technologies, Inc., Santa Clara, CA, USA). Immunohistochemistry (IHC) staining was performed on intelliPATH FLX (Biocare Medical, LLC, Pacheco, CA, USA) with Polymer Immunohistochemical Detection System (Wuxi OriGene Technologies, Inc., Wuxi, China, catalog number MA-2000). Primary antibodies, including anti-Calretinin, -Cytokeratin 5/6, -WT-1 and -Ki-67, were used for IHC analysis (Table 1). The images were captured using Zeiss Axio Scope.A1 and Mshot Microscopic Camera MS60. All HE and IHC sections were reviewed by 3 senior pathologists.

Establishment of MPM primary cell lines

Isolation and purification: The s.c. tumor was cut into 1 mm^3 pieces, which were then transferred to a centrifuge tube containing Dispase® II (neutral protease, grade II; Sigma, St. Louis, MO, USA) and digested on 37°C in-

cubator for 1 h. The cell suspension was filtered through a 70 μm cell filter into a 50 ml centrifuge tube, and was then centrifuged at 515 ×g for 5 min, followed by re-suspending in culture medium for culturing.

After 5 days of culturing, Dispase® II was added and incubated at 37°C for 10 min. Most tumor cells were detached from the flask bottom, while the fibroblasts were still adherent to the flask. The detached tumor cells were centrifuged at 515 ×g for 5 min and were re-suspended in culture medium for culturing.

Cell culture: Cells were cultured in DMEM containing 10% fetal bovine serum, 100 U/ml penicillin and 100 μg/ml streptomycin (penicillin-streptomycin-glutamine; Gibco) at 37°C, 5% CO_2 in a humidified Forma Steri-Cycle CO_2 Incubator (Thermo Fisher Scientific, Waltham, MA, USA).

Cell identification

Swiss-Giemsa staining: Sterile round slides were added onto the 24-well culture plate, and 200 μl culture medium was added into each well. Cells were diluted to the concentration of 1 × 10^6 cells/ml, and 30 μl of cell suspension was added to each well. After 24 h of incubation, cells were fixed by using ice-cold methanol for 3 min and were stained with Swiss-Giemsa (Solarbio, Beijing, China) for 5 min. The morphology of cells was observed under an EVOS™ XL Core Configured Microscope (Thermo Fisher Scientific).

Immunofluorescence staining: Cells were added to 24-well plate according to above method, fixed with ice-methanol for 5 min. Primary mouse anti-Calretinin monoclonal antibody (1F5H1, Abcam, Bristol, UK; 1:200) and anti-Cytokeratin 5 monoclonal antibody (XM26, Abcam; 1:250) were revealed with specific goat anti-mouse Alexa Fluor®555 (IgG H&L)-conjugated secondary antibodies (ab150114, Abcam; 1:1,000) for 30 min at 37°C. Nuclei were stained with 4',6-diamidino-2-phenylindole (DAPI; Beyotime Institute of Biotechnology, Beijing, China). Pictures were captured under a fluorescence microscope (BX43, Olympus, Chiba, Japan).

Study on the molecular pathology by whole-exome sequencing (WES)

The WES sequencing protocol prescribed by Giannakis *et al*. [17] was used in our study. In terms of models, the tumor tissues preserved in the liquid nitrogen were centrifuged with 1 min, the centrifugal rate of 9,400 ×g/min. For the patient, the formalin-fixed, paraffin-embedded tumor tissues were sectioned into 5 μm for sequencing, and the normal tissues adjacent to tumor were regarded as control. QIAGEN DNA kit (QIAGEN NV, Hilden, German) was used to extract genomic DNA, and the Quant-iT Pico Green dsDNA Assay Kit (Invitrogen/ThermoFisher Scientific) was conducted to check the DNA quality. The whole-exome capture libraries (final concentration >20 ng/μl) were constructed by shearing, end repair, phosphorylation and ligation to barcoded sequencing adaptors. SureSelectXT Human All Exon V6 (Agilent Technologies) was used to capture DNA and the Illumina X10 platform (Illumina Inc., San Diego, CA, USA) was then used to sequenced the samples. The method of MuTect [18] was performed to detect the somatic mutations, and the somatic cell insertion and deletion markers were detected by the method of Indelocator and Strelka [19]. The mutation analysis of WES data was performed using human genome build hg19 as the reference genome.

Statistical analysis

Data are presented as mean ± SD when normal distribution is satisfied. Statistical analyses and image processing were performed using GraphPad Prism 8.0.1 (GraphPad, San Diego, CA, USA) and Adobe Photoshop 2017 CC software (Adobe Systems, San Jose, CA, USA). Student's *t*-test were applied to evaluated statistical significance. $P<0.05$ was considered statistically significant.

Results

The characterization of subcutaneous MPM model

The growth curve of s.c. tumor at the 4th passage was shown in Fig. 2A. The volume of s.c. tumor reached 53.32 ± 10.01 mm^3 after day 18 of inoculation, the slow growth phase was from day 18 to 30, and the rapid growth phase lasted from day 30 to 54. The volume reached 498.31 ± 2.22 mm^3 on the day 54 of grafting. Microscopically, the HE results showed that the tumors from s.c. model were epithelioid mesothelioma (Fig. 2B), and the IHC results demonstrated that the expression of Calretinin and Ki-67 were both positive (Figs. 2C and D).

Establishment and pathological features of the new MPM PDX models

General status: From the day of grafting to autopsy, the general conditions of nude mice, such as diet, excretion, mental state, were normal. The body weight increased steadily from D1 to D6, followed by a plateau from D6 to D10, and then decreased since D10 to D14. Female and male nude mice had the same body weight change trend (Fig. 3A).

Gross pathology: On the 14th day of grafting, the mice were sacrificed to observe the situation of model estab-

 doi: 10.1538/expanim.20-0119

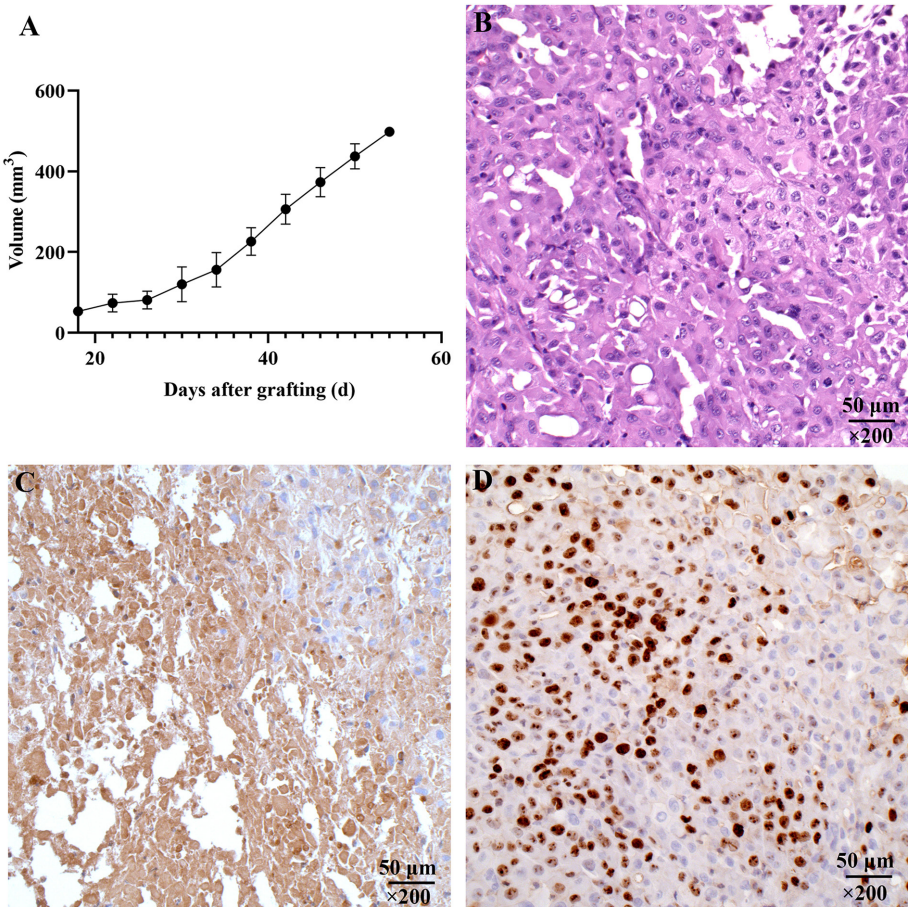

Fig. 2. The growth curve and histopathological results of malignant peritoneal mesothelioma (MPM) subcutaneous (s.c.) model. A, The growth curve of s.c. tumor; B, The hematoxylin-eosin (HE) staining of the s.c. model (B, ×200); C, The expression of Calretinin was positive (C, ×200); D, The expression of Ki-67 was positive (D, ×200).

lishment. The ePCI score (Fig. 3B) was used to quantify the tumor formation of MPM. The rate of model establishment was 100% (20/20). The tumors were white, single or fused, and invaded multiple organs, including the mesentery, 95% (19/20; Fig. 3C), diaphragm, 45% (9/20; Fig. 3D), liver, 50% (10/20), stomach, 40% (8/20), pancreas, 10% (2/20), spleen, 65% (13/20; Fig. 3E), kidney, 40% (8/20), and pelvic cavity, 100% (20/20; Fig. 3F). The ePCI score of female and male nude mice were 8.80 ± 1.75 and 9.20 ± 1.81 (P=0.6219; Fig. 3G; Table 2), respectively.

Histopathological study: The results of HE staining showed that the tumor tissue of nude mice was epithelioid mesothelioma. The tumor cells were morphologically diverse, large in size, markedly heteromorphic, and invaded multiple organs, such as diaphragm, liver (Figs. 4A and B), pancreas (Figs. 4C and D), spleen, kidney, mesentery (Figs. 4E and F), and uterus (Figs. 4G and H), which is consistent with that of the patient (Figs. 4I–L).

Immunohistochemical staining of the MPM PDX models showed that the Calretinin, Cytokeratin 5/6, WT-1 and Ki-67 were all positive (Figs. 5A–D). These results were also consistent with the patient (Figs. 5E–H).

Establishment and cytological characteristics of primary MPM cell lines

Swiss-Giemsa staining: The morphology of MPM cells under inverted phase contrast microscope was shown in Fig. 6A. Swiss-Giemsa staining was performed to reveal the diverse cell morphology, such as varying size, shape, nucleus number, and the visibility of nucleolus (Fig. 6B).

Immunofluorescence staining: The immunofluorescence staining was performed to confirm the expression of Calretinin and Cytokeratin 5 in the established MPM cells (Fig. 6C), which was in accordance with the cytological characteristics of epithelioid mesothelioma.

Potential molecular features of MPM PDX models

26 and 36 mutant genes with higher frequency (mutation abundance >10%) were found in PDX models and

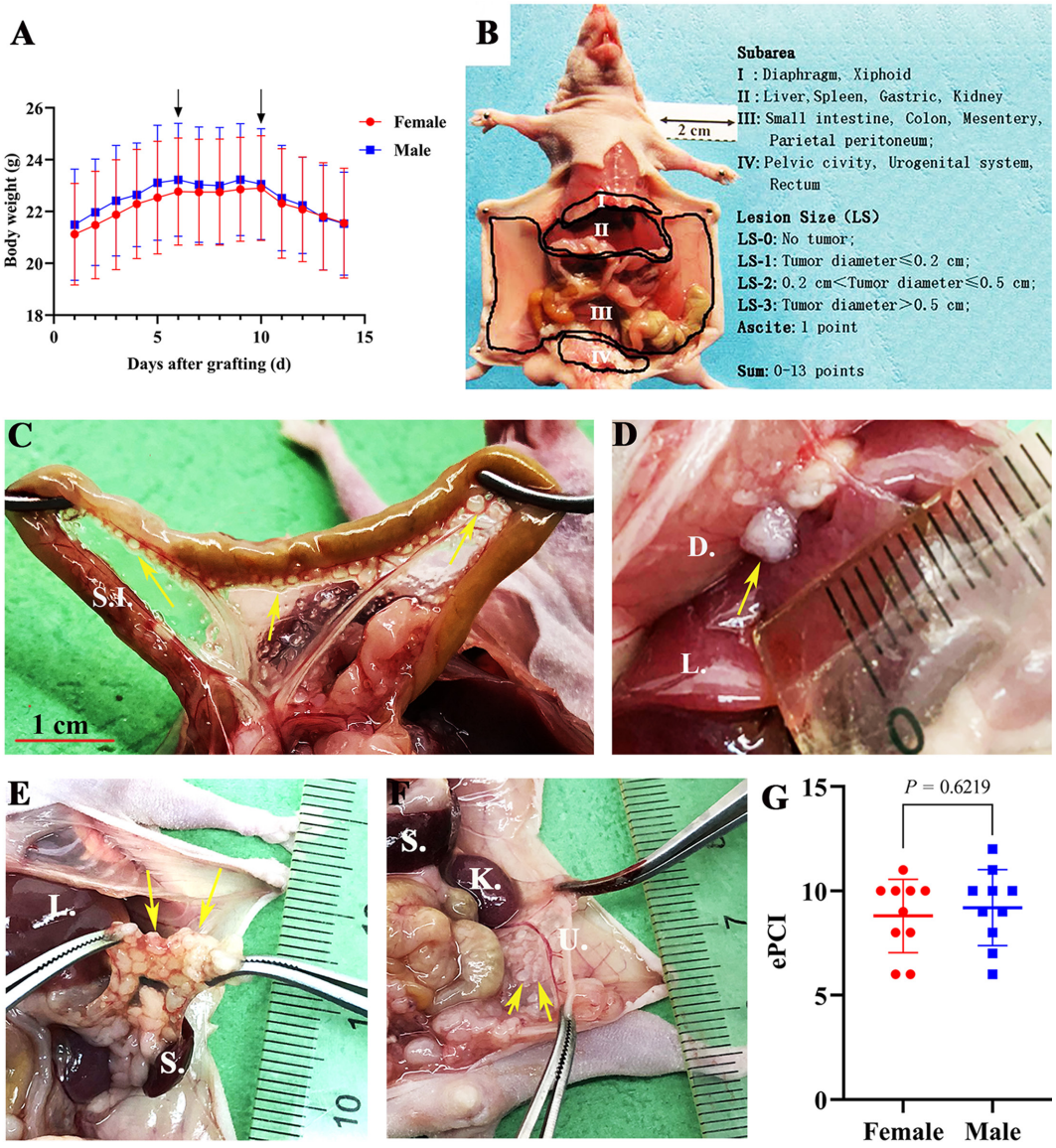

Fig. 3. Body weight change, experimental peritoneal cancer index (ePCI) score, and the gross pathology of the new malignant peritoneal mesothelioma (MPM) patient-derived xenograft (PDX) models. A, The body weight change of female and male nude mice; B, The subarea and scoring of ePCI score system [16]; C, The tumors invaded mesentery of the nude mice; D, Tumors invaded the diaphragm; E, Splenic mesentery of nude mice was invaded by tumors; F, The uterus of mice was invaded; G, ePCI score of female and male models. S.I., small intestine; D., diaphragm; L., liver; S., spleen; K., kidney; U., uterus.

the patient, respectively. 21 mutant genes were shared in the two groups, among them, the genes related to tumorigenesis and development including *BAP1*, *NF2*, *MTBP*, *NECTIN2*, *CDC23*, *LRPPRC*, *TRIM25*, and *DHRS2*(Table 3).

Discussion

By using surgical specimens collected from MPM patient, we established PDX models and primary cell lines of MPM, which highly replicated the pathological development of clinical patients. The biological behaviors of the PDX models were characterized by highly malignant potential and strong invasion and metastasis behavior. Tumors invaded multiple organs, including diaphragm, liver, spleen, kidney, mesentery, and organs of pelvic cavity. The histopathological results also showed that the pathological features of the models and primary cell lines were epithelioid mesothelioma, consistent with that of the patient. Therefore, the established PDX models and primary cancer cell lines provided a platform for *in vivo* and *in vitro* studies of the pathological mechanism and the clinical intervention for MPM.

Both the reported PDX models of malignant pleural mesothelioma [13] and our MPM PDX models are de-

Table 2. The ePCI score of MPM PDX models

Sex	The organs invaded by tumor in each subarea				Ascites	ePCI score
	I	II	III	IV		
Female	Diaphragm; The largest tumor diameter was 0.1 cm; LS-1	Liver, kidney and spleen; The largest tumor diameter was 0.3 cm; LS-2	Mesentery; The largest tumor diameter was 0.3 cm; LS-2	Pelvis, uterus; The largest tumor diameter was 0.7 cm; LS-3	No; LS-0	8
Female	No; LS-0	Liver, spleen; The largest tumor diameter was 0.9 cm; LS-3	Small intestine, mesentery; The largest tumor diameter was 0.6 cm; LS-3	Pelvis, uterus; The largest tumor diameter was 0.6 cm; LS-3	No; LS-0	9
Female	Diaphragm; The largest tumor diameter was 0.1 cm; LS-1	Liver; The largest tumor diameter was 0.8 cm; LS-3	Mesentery; The largest tumor diameter was 0.6 cm; LS-3	Pelvis; The largest tumor diameter was 0.8 cm; LS-3	Bloody ascites; LS-1	11
Female	Diaphragm; The largest tumor diameter was 0.1 cm; LS-1	Liver, kidney and spleen; The largest tumor diameter was 0.4 cm; LS-2	Mesentery; The largest tumor diameter was 0.6 cm; LS-3	Pelvis, uterus; The largest tumor diameter was 1.0 cm; LS-3	Bloody ascites; LS-1	10
Female	Diaphragm; The largest tumor diameter was 0.2 cm; LS-1	Liver, kidney and spleen; The largest tumor diameter was 0.7 cm; LS-3	Colon and mesentery; The largest tumor diameter was 0.5 cm; LS-2	Pelvis, uterus; The largest tumor diameter was 0.8 cm; LS-3	Bloody ascites; LS-1	10
Female	Diaphragm; The largest tumor diameter was 0.2 cm; LS-1	Kidney and spleen; The largest tumor diameter was 0.6 cm; LS-3	Colon and mesentery; The largest tumor diameter was 0.8 cm; LS-3	Pelvis, uterus; The largest tumor diameter was 1.2 cm; LS-3	No; LS-0	10
Female	No; LS-0	Spleen; The largest tumor diameter was 0.4 cm; LS-2	Mesentery; The largest tumor diameter was 0.1 cm; LS-1	Pelvis; The largest tumor diameter was 0.9 cm; LS-3	No; LS-0	6
Female	No; LS-0	Spleen; The largest tumor diameter was 0.8 cm; LS-3	Mesentery; The largest tumor diameter was 0.2 cm; LS-1	Pelvis, uterus; The largest tumor diameter was 0.3 cm; LS-2	No; LS-0	6
Female	No; LS-0	Kidney and spleen; The largest tumor diameter was 0.9 cm; LS-3	Mesentery; The largest tumor diameter was 0.6 cm; LS-3	Pelvis, uterus; The largest tumor diameter was 0.9 cm; LS-3	Bloody ascites; LS-1	10
Female	Diaphragm; The largest tumor diameter was 0.1 cm; LS-1	Liver; The largest tumor diameter was 0.4 cm; LS-2	Mesentery; The largest tumor diameter was 0.3 cm; LS-2	Pelvis; The largest tumor diameter was 0.6 cm; LS-3	No; LS-0	8
Male	Diaphragm; The largest tumor diameter was 0.4 cm; LS-2	Liver; The largest tumor diameter was 0.3 cm; LS-2	Mesentery; The largest tumor diameter was 0.8 cm; LS-3	Pelvis; The largest tumor diameter was 1.0 cm; LS-3	No; LS-0	10
Male	No; LS-0	Liver and kidney; The largest tumor diameter was 0.8 cm; LS-3	Mesentery; The largest tumor diameter was 0.8 cm; LS-3	Pelvis; The largest tumor diameter was 0.7 cm; LS-3	Bloody ascites; LS-1	10
Male	Diaphragm; The largest tumor diameter was 0.2 cm; LS-1	Liver; The largest tumor diameter was 0.6 cm; LS-3	Colon; The largest tumor diameter was 0.6 cm; LS-3	Pelvis; The largest tumor diameter was 0.3 cm; LS-2	Bloody ascites; LS-1	10
Male	No; LS-0	Liver and spleen; The largest tumor diameter was 0.5 cm; LS-2	Mesentery; The largest tumor diameter was 0.8 cm; LS-3	Pelvis; The largest tumor diameter was 1.1 cm; LS-3	Bloody ascites; LS-1	9
Male	Diaphragm; The largest tumor diameter was 0.3 cm; LS-2	Liver and spleen; The largest tumor diameter was 1.4 cm; LS-3	Colon and mesentery; The largest tumor diameter was 0.7 cm; LS-3	Pelvis; The largest tumor diameter was 0.8 cm; LS-3	Bloody ascites; LS-1	12
Male	Diaphragm; The largest tumor diameter was 0.3 cm; LS-2	Spleen; The largest tumor diameter was 0.7 cm; LS-3	Mesentery; The largest tumor diameter was 0.3 cm; LS-2	Pelvis; The largest tumor diameter was 1.2 cm; LS-3	Bloody ascites; LS-1	11
Male	No; LS-0	Spleen; The largest tumor diameter was 0.5 cm; LS-2	Mesentery; The largest tumor diameter was 0.7 cm; LS-3	Pelvis; The largest tumor diameter was 0.1 cm; LS-1	No; LS-0	6
Male	No; LS-0	Spleen and kidney; The largest tumor diameter was 0.5 cm; LS-2	Mesentery; The largest tumor diameter was 0.6 cm; LS-3	Pelvis; The largest tumor diameter was 0.8 cm; LS-3	Bloody ascites; LS-1	9
Male	No; LS-0	Spleen and kidney; The largest tumor diameter was 0.2 cm; LS-1	Mesentery; The largest tumor diameter was 0.8 cm; LS-3	Pelvis; The largest tumor diameter was 0.7 cm; LS-3	No; LS-0	7
Male	No; LS-0	Liver and kidney; The largest tumor diameter was 0.3 cm; LS-2	Mesentery; The largest tumor diameter was 0.8 cm; LS-3	Pelvis; The largest tumor diameter was 0.6 cm; LS-3	No; LS-0	8

MPM, malignant peritoneal mesothelioma; PDX, patient-derived xenograft; ePCI, experimental peritoneal cancer index.

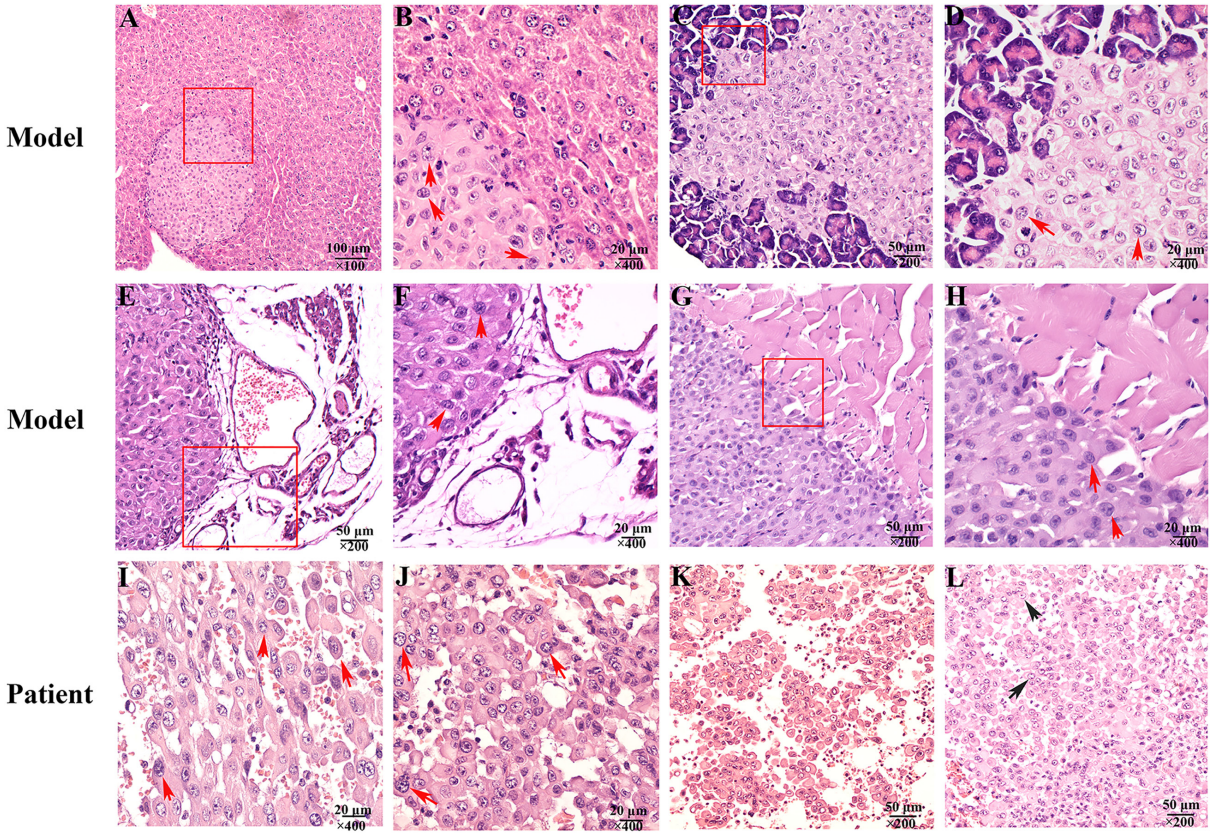

Fig. 4. The hematoxylin-eosin (HE) staining of the malignant peritoneal mesothelioma (MPM) patient-derived xenograft (PDX) models and the patient. A&B, The tumors of models invaded the liver (A, ×100), the tumor cells were morphologically diverse, large in size, and markedly heteromorphic (B, ×400; red arrow); C&D, The tumors of models invaded the pancreas (C, ×200), and the tumor cells were markedly heteromorphic (D, ×400; red arrow); E&F, The tumors of models invaded the mesentery (E, ×100), the tumor cells were characterized by atypia (F, ×400; red arrow); G&H, The tumors of models invaded the uterus (G, ×200), and the tumor cells were atypia (H, ×400; red arrow); I&J, The HE staining of the patient showed the tumor cells were also markedly heteromorphic (I&J, ×400; red arrow) [25]; K, The tumor cells of patient were arranged in a papillary structure (K, ×200) [25]; L, The tumor cells of patient were of clear cell type, and their cytoplasm was translucent (L, ×200; black arrow) [25].

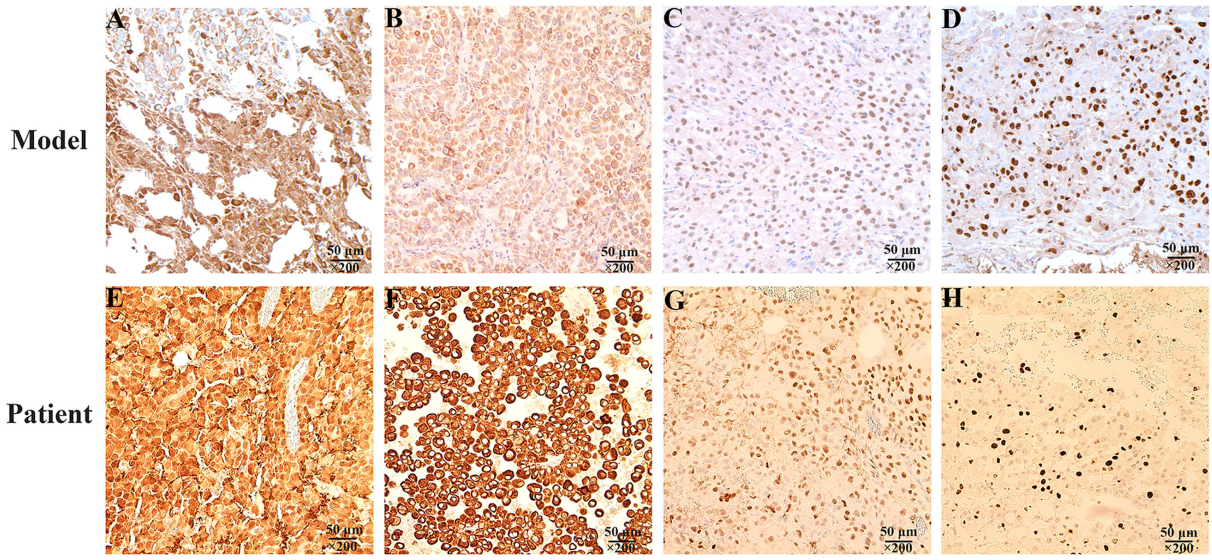

Fig. 5. The immunohistochemical staining of the malignant peritoneal mesothelioma (MPM) patient-derived xenograft (PDX) models and the patient. A, The Calretinin of the tumor tissues of the models was positive, with the nucleus and cytoplasm stained; B, The Cytokeratin 5/6 of the models was positive; C, The WT-1 of the models was positive; D, The Ki-67 of the models was positive, with the nucleus stained; E, The Calretinin of the patient was positive [25]; F, The Cytokeratin 5/6 of the patient was positive [25]; G, The WT-1 of the patient was positive [25]; H, The Ki-67 of the patient was positive, (A–H, ×200) [25].

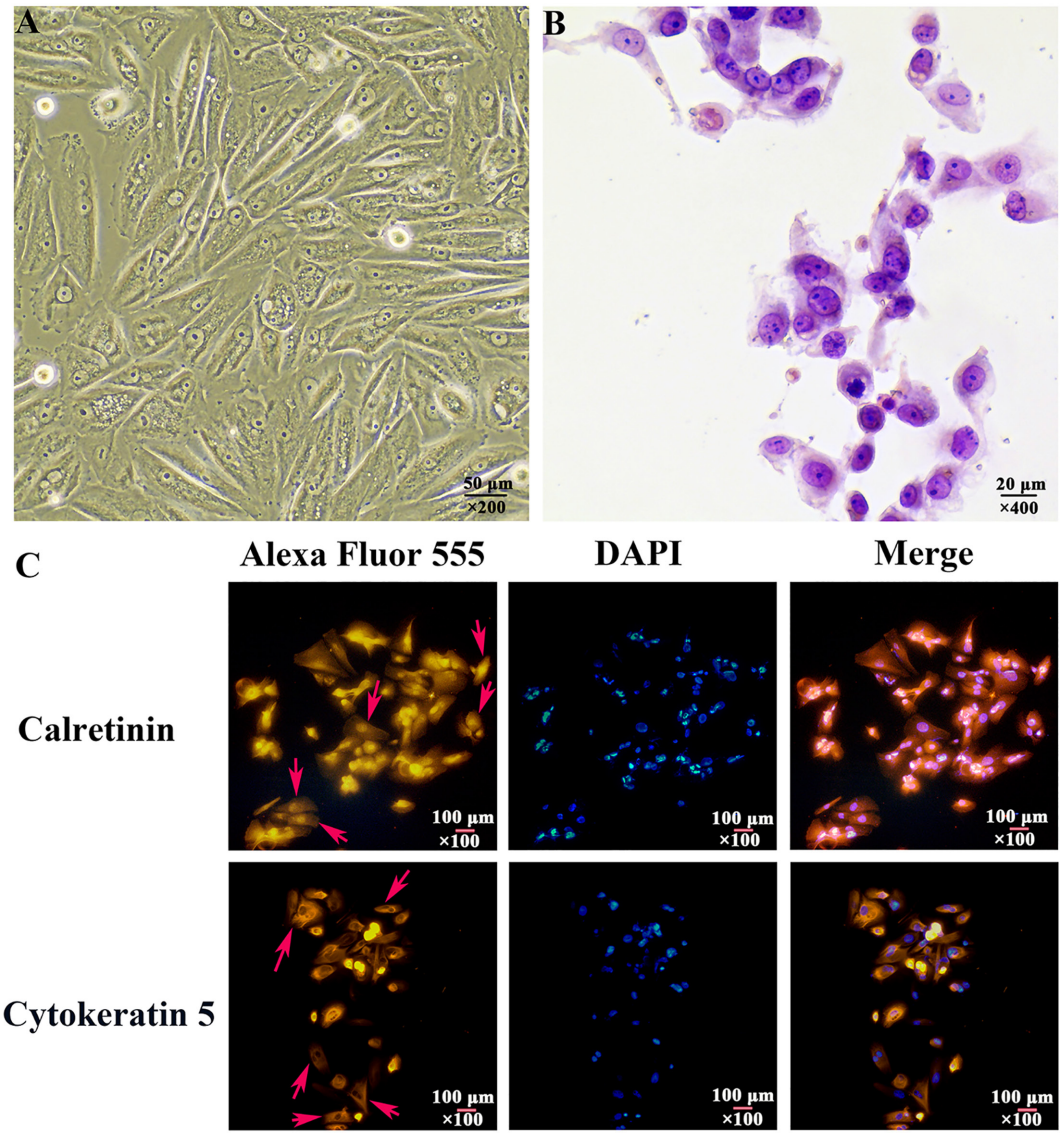

Fig. 6. Cytological characteristics of primary malignant peritoneal mesothelioma (MPM) cell lines. A, MPM cells morphology was showed under the inverted phase contrast microscope (A, ×200); B, The diverse cell morphology was revealed by Swiss-Gimsa staining (B, ×400); C, The immunofluorescence staining showed that the expression of Calretinin was located on both nucleus and cytoplasm, and the expression of Cytokeratin 5 was located on the cytoplasm (C, ×100; red arrow).

Table 3. Gene mutations related to tumor shared between the models and the patient

Gene	Mutation Abundance (%)	Type of mutation	Exon	Base mutation	Amino acids mutation
BAP1	99.9	FM	13	c.1464delC	p.P488fs
NF2	90.0	FM	5	c.484delT	p.F162fs
MTBP	60.3	FM	2	c.144delC	p.H48fs
NECTIN2	56.6	SNV	3	c.619A>T	p.T207S
CDC23	48.9	SNV	13	c.1421C>G	p.A474G
LRPPRC	47.2	FM	20	c.1978dupA	p.T660fs
TRIM25	33.7	SNV	4	c.998T>C	pL333P
DHRS2	32.1	SNV	8	c.722G>A	p.R241K

FM, frameshift mutation; SNV, single nucleotide mutation.

rived from surgical tissues, and replicate the clinical spreading of the patient's disease, however, we also use the ePCI score to quantify the tumor formation of MPM PDX models, and conduct molecular pathology research on these models to discover the genetic changes in MPM.

By observing the body weight change trend of nude

mice during grafting, we found that the plateau was appeared on D6, and the body weight decreased on D10, which was not affected by gender. The body weight change suggested that the PDX tumors had an impact on the general state of nude mice on D6 of grafting, and the nude mice were in a consumption state on D10. Therefore, the body weight change during the grafting was of reference significance in judging the impact of tumors on the host and the biological behavior of the tumors. Moreover, the ePCT score of female and male nude mice also indicated that gender did not affect the establishment of models.

Although the established MPM PDX models have the same immuno-profile as the patient, the expression of Calretinin, Cytokeratin 5/6, WT-1 and Ki-67 in tumor tissue of the patient were stronger than that in the models. The reasons may be as follows: 1) Tumor heterogeneity occurred during the passage in nude mice, 2) Tumor cells from different sites had various proliferation ability and malignant potentials.

In terms of molecular pathology research, 21 genes with high mutation abundance were shared between the PDX models and the patient. The genes associated with tumorigenesis and development include BAP1, NF2, MTBP, and NECTIN2. Both BAP1 and NF2 were frameshift mutations, with mutation abundances of 99.9% and 90.0%, respectively. Evidence previously reported that mutations or deletions of BAP1 and NF2 were found in malignant mesothelioma, with the mutation abundances of 57% and 35%, respectively, NF2 mutations or deletions were associated with poor prognosis, and provided a new target for MPM, while the relationship between the mutation of BAP1 and the prognosis in MPM patients was still controversial [20]. NECTIN2 was an adhesion molecule that played an important role in tumor growth and metastasis. In addition, NECTIN2 was also a ligand of NK cell activating receptor CD226 and highly expressed in colon cancer tissues. Upregulating the expression intensity of NECTIN2 in colon cancer tissues can activate the killing effect of NK cells [21, 22]. However, the function of NECTIN2 mutation in MPM are unclear. Moreover, the mutant genes between the established models and the patient were not completely identical, 5 mutant genes were only existed in models, and 15 mutant genes in patient. The causes could be the following: (1) Tumor heterogeneity led to the different mutant genes between the two groups, (2) The tumor tissues sequenced in the patient were paraffin section, while the models were fresh frozen tissues, which may led to the different results, and (3) The genes of the models may have changed due to the environment factors during the passaging process. However, the established PDX models still share the key genes and can conduct related studies.

Some animal models and few primary cell lines of MPM have been reported. Feng *et al.* [23] inoculated mesothelioma cell lines NCI-H226 into the abdominal cavity of 6-week-old female NCr-nu/nu nude mice to establish an MPM model, and conducted drug intervention study. The tumors invaded the diaphragm, liver, pancreas, and peritoneum of nude mice. Yang *et al.* [24] inoculated a AB12 cell line, a malignant pleural mesothelioma cell line, into 5-week-old female BALB/C nude mice to form a subcutaneous tumor model. They observed the changes in tumor volume and weight of this model to determine the efficacy of drugs. However, few primary cell lines of MPM have been reported. Compared with the existing MPM models, our established models have the following characteristics: (1) Using MPM surgical specimens to directly grafted nude mice to establish the MPM PDX models, this method not only saved time and cost, but also simulated maximally the tumor biological behavior of the clinical patients; (2) The established PDX models exhibited the pathological features highly consistent with the clinicopathological characteristics of MPM in terms of gross pathology and histopathology; and (3) The PDX models own the key mutant genes for the development of MPM, which may become a research tool for exploring the mechanism and new therapeutic targets for MPM. In addition, we also cultured primary MPM cell lines derived from the established subcutaneous models, and thus provided a platform *in vitro* study.

In conclusion, we established PDX models and primary cell lines to recapitulate the biological characteristics of MPM and provided a novel and promising platform for *in vivo* and *in vitro* study on MPM.

Author Contributions

YZR was involved in research concept and design, collection data, data analysis and interpretation, and manuscript preparation. CZG was involved in research concept and design. JZH, LYL, ZJ, MR, LZ, JX were involved in collection data. CQ, DXM and LY were contributed to research design, data analysis and interpretation, manuscript revision and final approval.

Conflicts of Interests

The authors declare that they have no competing interests.

Acknowledgments

This study was supported by funding from Beijing Municipal Administration of Hospitals' Ascent Plan (DFL20180701); General Program of National Natural Science Foundation of China (82073376); Beijing Municipal Grant for Medical Talents Group on Peritoneal Surface Oncology (2017400003235J007).

References

1. Price B. Analysis of current trends in United States mesothelioma incidence. Am J Epidemiol. 1997; 145: 211–218. [Medline] [CrossRef]
2. Kaya H, Sezgı C, Tanrıkulu AC, Taylan M, Abakay O, Sen HS, et al. Prognostic factors influencing survival in 35 patients with malignant peritoneal mesothelioma. Neoplasma. 2014; 61: 433–438. [Medline] [CrossRef]
3. Feldman AL, Libutti SK, Pingpank JF, Bartlett DL, Beresnev TH, Mavroukakis SM, et al. Analysis of factors associated with outcome in patients with malignant peritoneal mesothelioma undergoing surgical debulking and intraperitoneal chemotherapy. J Clin Oncol. 2003; 21: 4560–4567. [Medline] [CrossRef]
4. Sugarbaker PH, Yan TD, Stuart OA, Yoo D. Comprehensive management of diffuse malignant peritoneal mesothelioma. Eur J Surg Oncol. 2006; 32: 686–691. [Medline] [CrossRef]
5. Yano H, Moran BJ, Cecil TD, Murphy EM. Cytoreductive surgery and intraperitoneal chemotherapy for peritoneal mesothelioma. Eur J Surg Oncol. 2009; 35: 980–985. [Medline] [CrossRef]
6. Hompes D, D'Hoore A, Van Cutsem E, Fieuws S, Ceelen W, Peeters M, et al. The treatment of peritoneal carcinomatosis of colorectal cancer with complete cytoreductive surgery and hyperthermic intraperitoneal peroperative chemotherapy (HIPEC) with oxaliplatin: a Belgian multicentre prospective phase II clinical study. Ann Surg Oncol. 2012; 19: 2186–2194. [Medline] [CrossRef]
7. Bretcha-Boix P, Farré-Alegre J, Sureda M, Dussan C, Pérez Ruixo JJ, Brugarolas Masllorens A. Cytoreductive surgery and perioperative intraperitoneal chemotherapy in patients with peritoneal carcinomatosis of colonic origin: outcomes after 7 years' experience of a new centre for peritoneal surface malignancies. Clin Transl Oncol. 2010; 12: 437–442. [Medline] [CrossRef]
8. De Nardo P. [Veterinary environmental epidemiology: the case of respiratory pathology in the dog]. Ann Ist Super Sanita. 1997; 33: 587–593. [Medline]
9. Kim JH, Choi YK, Yoon HY, Kweon OK, Kim DY. Juvenile malignant mesothelioma in a dog. J Vet Med Sci. 2002; 64: 269–271. [Medline] [CrossRef]
10. Wagner JC, Berry G. Mesotheliomas in rats following inoculation with asbestos. Br J Cancer. 1969; 23: 567–581. [Medline] [CrossRef]
11. Colt HG, Astoul P, Wang X, Yi ES, Boutin C, Hoffman RM. Clinical course of human epithelial-type malignant pleural mesothelioma replicated in an orthotopic-transplant nude mouse model. Anticancer Res. 1996; 16: 633–639. [Medline]
12. Astoul P, Boutin C. [An experimental model of pleural cancer. Value of orthotopic implantation of human tumor tissue in nude mice]. Rev Mal Respir. 1997; 14: 355–362. [Medline]
13. Astoul P, Wang X, Colt H, Boutin C, Hoffman R. A patient-like human malignant pleural mesothelioma nude-mouse model. Oncol Rep. 1996; 3: 483–487. [Medline]
14. Enomoto Y, Kasai T, Takeda M, Takano M, Morita K, Kadota E, et al. A comparison of epidermal growth factor receptor expression in malignant peritoneal and pleural mesothelioma. Pathol Int. 2012; 62: 226–231. [Medline] [CrossRef]
15. Enomoto Y, Kasai T, Takeda M, Takano M, Morita K, Kadota E, et al. Epidermal growth factor receptor mutations in malignant pleural and peritoneal mesothelioma. J Clin Pathol. 2012; 65: 522–527. [Medline] [CrossRef]
16. Lin YL, Zhang J, Yan FC, Jiang X, Ma R, Yang ZR, et al. Establishment of patient-derived xenograft model of peritoneal mucinous carcinomatosis with signet ring cells and in vivo study on the efficacy and toxicity of intraperitoneal injection of 5-fluorouracil. Cancer Med. 2020; 9: 1104–1114. [Medline] [CrossRef]
17. Giannakis M, Mu XJ, Shukla SA, Qian ZR, Cohen O, Nishihara R, et al. Genomic correlates of immune-cell infiltrates in colorectal carcinoma. Cell Rep. 2016; 17: 1206. [Medline] [CrossRef]
18. Cibulskis K, Lawrence MS, Carter SL, Sivachenko A, Jaffe D, Sougnez C, et al. Sensitive detection of somatic point mutations in impure and heterogeneous cancer samples. Nat Biotechnol. 2013; 31: 213–219. [Medline] [CrossRef]
19. Saunders CT, Wong WS, Swamy S, Becq J, Murray LJ, Cheetham RK. Strelka: accurate somatic small-variant calling from sequenced tumor-normal sample pairs. Bioinformatics. 2012; 28: 1811–1817. [Medline] [CrossRef]
20. Singhi AD, Krasinskas AM, Choudry HA, Bartlett DL, Pingpank JF, Zeh HJ, et al. The prognostic significance of BAP1, NF2, and CDKN2A in malignant peritoneal mesothelioma. Mod Pathol. 2016; 29: 14–24. [Medline] [CrossRef]
21. Bekes I, Löb S, Holzheu I, Janni W, Baumann L, Wöckel A, et al. Nectin-2 in ovarian cancer: How is it expressed and what might be its functional role? Cancer Sci. 2019; 110: 1872–1882. [Medline] [CrossRef]
22. Molfetta R, Milito ND, Zitti B, Lecce M, Fionda C, Cippitelli M, et al. The Ubiquitin-proteasome pathway regulates Nectin2/CD112 expression and impairs NK cell recognition and killing. Eur J Immunol. 2019; 49: 873–883. [Medline] [CrossRef]
23. Feng M, Zhang J, Anver M, Hassan R, Ho M. In vivo imaging of human malignant mesothelioma grown orthotopically in the peritoneal cavity of nude mice. J Cancer. 2011; 2: 123–131. [Medline] [CrossRef]
24. Yang H, Wang Y, Cheryan VT, Wu W, Cui CQ, Polin LA, et al. Withaferin A inhibits the proteasome activity in mesothelioma in vitro and in vivo. PLoS One. 2012; 7: e41214. [Medline] [CrossRef]
25. Yang ZR, Lin YL, Zhang J, Ma R, Li Z, Jiang X, et al. [Establishment and characterization of patient derived xenograft model of malignant peritoneal mesothelioma in nude mice]. Zhonghua Bing Li Xue Za Zhi. 2020; 49: 162–167. [Medline]